Improved symmetry analysis of many-moded microstructure optical fibers

John M. Fini

OFS Labs, Murray Hill, New Jersey 07974

Received October 17, 2003; revised manuscript received March 19, 2004; accepted April 5, 2004

Various methods for simulating microstructure fibers have incorporated symmetry for improved efficiency and discrimination of nearly degenerate modes. A revision of the previously used symmetry-class implementations is proposed, with a more efficient partition of the degenerate classes. Advantages demonstrated using a multipole calculation should apply to finite-element and other simulation methods. © 2004 Optical Society of America

OCIS codes: 060.2280, 230.3990.

1. INTRODUCTION

Microstructure fibers, initially discussed some time ago,[1,2] have recently captured the interest and imagination of the community and have made rapid strides forward.[3–5] Many interesting microstructure optical fiber (MOF) results have so far involved fibers with only one or a few guided modes. Supercontinuum generation effects[6] and endlessly single-mode operation,[3] for example, can be understood by modeling only the fundamental mode of fibers with a small number of cladding holes. Scalar numerical results have proven useful in some cases.[7]

While simple single-mode models have often been sufficient in understanding MOF propagation, interest is now turning to structures where multiple modes and more detailed fiber geometries are essential. Low-loss guidance in air-core fibers,[4] for example, requires many cladding holes and precise core shape. Air-core propagation can be deteriorated by multiple unwanted surface modes localized in glass webs near the core.[8] Other applications, such as sensor fibers and multicore couplers, similarly involve multiple, nearly degenerate modes.

For these reasons, the cleanest possible separation of mode classes using symmetry is desirable. It not only improves efficiency by reducing the size of matrix calculations, but can avoid qualitative inaccuracies.[9,10] For this reason, most theory and modeling efforts include symmetry analysis in some form. However, in most microstructure fiber simulations described so far, symmetry classes have not been interpreted in the most efficient way.

In this paper, a revised implementation of symmetry classes is proposed for the most common waveguides, with C_{6v} (sixfold rotational and reflection) symmetry. The partitioning of degenerate modes into classes can be done in different ways; as we will see, the most efficient partitioning starts with a simple separation into rotational symmetry classes. This is easily implemented and cleanly separates the degenerate symmetry classes. Nondegenerate mode classes, which have both rotational and reflection symmetry, are not redefined since previous implementations are already quite efficient.

The suggested symmetry analysis has already been used in some previous simulations, where its application was fairly straightforward.[2,10] The present results show that they can be applied more broadly to other methods, where the implementation is less obvious. The multipole method is implemented in the following simulations, but comments are provided that should be useful for other methods as well.

The last section presents a simulation of a fiber with rotational symmetry only, which fundamentally cannot use the C_{6v} symmetry classes. These are efficiently handled by the revised multipole method with no additional changes. This demonstrates that some additional design flexibility is opened up by the revised method at a minimal cost of efficiency.

2. GUIDED MODES AND SYMMETRY

Microstructure fibers have complex geometry with features of the order of the wavelength of light, and so modeling of light propagation in these fibers is nontrivial. Several methods have been developed, with various assumptions and trade-offs. While beam-propagation and finite-difference time-domain calculations have their place, most methods aim to find the guided eigenmodes of the waveguide: fields with characteristic wavelength λ and longitudinal wave number k_z,

$$\mathbf{E}(\mathbf{r}) = \mathbf{E}(x, y)\exp(ik_z z), \tag{1}$$

$$\mathbf{H}(\mathbf{r}) = \mathbf{H}(x, y)\exp(ik_z z). \tag{2}$$

Since modes are often leaky, k_z may have a small imaginary part and still describe a mostly confined mode with finite loss. For each numerical method, the field vectors are represented by a vector of coefficients $\mathbf{b}$, and Maxwell's equations reduce to a mode equation linear in $\mathbf{b}$.

For example, according to the finite-element method,[11] the vector $\mathbf{b}$ contains values of the magnetic field vector

sampled at many judiciously chosen grid points. The mode equation takes the form of an eigenvalue equation,

$$(\mathbf{A} - n_{\mathrm{eff}}^2\mathbf{B})\mathbf{b} = 0. \tag{3}$$

Similarly, eigenvalue-type mode equations can be obtained assuming $\mathbf{b}$ is a vector of coefficients for some set of basis functions. Depending on the basis, one can get the plane-wave expansion method[12] or the efficient modal method.[7]

Along slightly different lines, the multipole and boundary-element methods take advantage of the specific structure common to most MOFs. Assuming that the complex geometry is composed of homogeneous, constant-dielectric regions, these methods represent the mode field using a much smaller number of coefficients than the more general, "brute-force" approaches. The mode condition now takes a null-matrix form,

$$\mathbf{M}(\lambda, n_{\mathrm{eff}})\mathbf{b} = 0. \tag{4}$$

For the multipole method, $\mathbf{b}$ includes the coefficients of a circular-function expansion of the fields locally around each hole.[13] For the boundary-element method, like the finite-element method, $\mathbf{b}$ includes samples of the magnetic field, but here only samples on the boundaries of the constant-dielectric regions are needed.[14]

In all cases, symmetry allows dramatic simplification of the calculation. If the mode field has a symmetry, the full vector of coefficients $\mathbf{b}$ can be obtained from a much smaller set of coefficients $\mathbf{b}_s$ using the appropriate symmetry relations. This can be expressed generally using a sparse decoding matrix $\mathbf{Z}$ that is tall and thin:

$$\mathbf{b} = \mathbf{Z}\mathbf{b}_s. \tag{5}$$

Table 1 sketches the symmetry relations that could be used for the various methods, assuming, for example, a mode with sixfold rotational symmetry number p,

$$\mathbf{E}(\mathbf{R}_{\pi/3}\mathbf{r}) = \exp(ip\pi/3)\mathbf{R}_{\pi/3}\mathbf{E}(\mathbf{r}). \tag{6}$$

Here $\mathbf{R}_{\pi/3}$ rotates vectors by $\pi/3$ about the z axis. We note that for each simulation method, only some of the field components are explicitly represented (the remaining components can be derived using Maxwell's equations). For example, E_z and H_z might be explicitly represented in one implementation of the multipole method, but H_x and H_y might be represented for the boundary-element method. Table 1 is meant to give the general idea, but details of the symmetry relations depend on whether longitudinal or transverse fields are used. From these relations, one can obtain (roughly) six elements of $\mathbf{b}$ for each element of the reduced representation $\mathbf{b}_s$. Each element of the matrix $\mathbf{Z}$ is obtained in a straightforward way from the symmetry relations. The matrix typically has dimensions roughly $N \times (N/6)$ with only 1 or 2 nonzero elements per row. It is thus very easy to precompute, store, and multiply.

The modal conditions can be converted into a matrix equation of much smaller dimension once a reduced representation is defined. Specifically, the eigenvalue equation (3) becomes

$$\mathbf{Z}^*(\mathbf{A} - n_{\mathrm{eff}}^2\mathbf{B})\mathbf{Z}\mathbf{b}_s = (\mathbf{A}_s - n_{\mathrm{eff}}^2\mathbf{B}_s)\mathbf{b}_s = 0, \tag{7}$$

and the null-matrix equation (4) becomes

$$\mathbf{Z}^*\mathbf{M}\mathbf{Z}\mathbf{b}_s = \mathbf{M}_s\mathbf{b}_s = 0. \tag{8}$$

Here, the matrix $\mathbf{Z}^*$ can be chosen in a number of ways but generally projects a reduced vector of size $\sim N/6$ from a full vector $\mathbf{b}$ of size N. Typically one can choose an obvious, sparse inverting matrix, so that $\mathbf{Z}^*\mathbf{Z} = 1$ is the identity matrix with the dimension of $\mathbf{b}_s$.

3. REVISING C_{6v} SYMMETRY CLASSES

Previous discussions of symmetry in multipole MOF modeling[9,13] borrow from the general theory presented by McIsaac for electromagnetic waveguides.[15] Of course, the symmetry classes presented for C_{6v} waveguides are correct, but they do not take full advantage of the freedom we have in partitioning degenerate mode classes. This previous method[13] defines (arbitrarily) each degenerate mode class to have a definite reflection symmetry, but to have rotation symmetry only in superpositions. This results in making the quadrant a minimum computational sector: field values in one quadrant are represented explicitly, and the other sectors are inferred using even or odd symmetry of the mode upon reflection across the x and y axis.

It is possible instead to partition classes with definite rotational symmetry (but with reflection symmetry only in superpositions). In this case, the computational sector can be reduced to one sixth of the plane (or smaller) for both degenerate and nondegenerate modes, with corresponding reduction of the dimension of the modal equation (8). These advantages may seem natural in light of methods for modeling Bragg fibers[2] and other waveguide structures.[16] In fact, rotational symmetry has been applied to microstructure fibers using at least one method,[10] where the basis makes this a particularly natural choice. However, broader application to multipole and other modeling methods has not yet been reported.

Table 1. Symmetry Relations Used to Obtain Compact Field Representations for Various Methods Outlined[a]

Method	Coefficient Definition	Symmetry Relation
FE or BE	$H_{[x/y]}(\mathbf{r}_j) = b_j^{[x/y]}$	$\begin{pmatrix} b_{j'}^x \\ b_{j'}^y \end{pmatrix} = \exp(ip\pi/3)\mathbf{R}_{\pi/3}\begin{pmatrix} b_j^x \\ b_j^y \end{pmatrix}$
Multipole	$H_z(\mathbf{r}) = \Sigma_{j,m} b_m^{H,j} f_m(\mathbf{r} - \mathbf{r}_j)$	$b_m^{H,j'} = \exp[i(p-m)\pi]/3 b_m^{H,j}$
Plane Wave	$H_z(\mathbf{r}_j) = \Sigma_j b_j^H \exp(i\mathbf{k}_j \cdot \mathbf{r})$	$b_j^H = \exp(ip\pi)/3 b_j^H$

[a] In the expressions, we assume $\mathbf{r}_{j'} = \mathbf{R}_{\pi/3}\mathbf{r}_j$ and $\mathbf{k}_{j'} = \mathbf{R}_{\pi/3}\mathbf{k}_j$.

A. Simple Symmetry Arguments

McIsaac presents the symmetry classes in the difficult language of irreducible representations of the symmetry group. This is appropriate for a rigorous discussion but obscures some intuitive and easily derived properties of the modes. Consider a waveguide with N-fold rotational symmetry (made of isotropic dielectric). If fields $\mathbf{E}$ and $\mathbf{H}$ satisfy Maxwell's equations with a fixed wavelength λ and waveguide propagation constant k_z, then a rotation of these fields by $2\pi/N$ is also a valid solution with the same λ and k_z. We can define projection operators that partition the space into sectors according to rotation number l:

$$P_l\{\mathbf{E}(\mathbf{r})\} = \frac{1}{N}\sum_{n=1}^{N-1} \exp(-i2\pi nl/N) R_{2\pi/N}^{-n}\mathbf{E}(R_{2\pi/N}^{n}\mathbf{r}), \tag{9}$$

where $R_{2\pi/N}$ is the operator that applies the rotation to the fields. Since rotation preserves λ and k_z, the projection of any guided mode on sector l gives either zero or a valid confined inode with the same λ, k_z, and rotational symmetry number l.

Since the N projections together span the space, the projected modes include all guided modes, and the partition by rotation number is complete, *regardless* of whether a waveguide has reflection symmetry. Thus the minimum computational sector for an eigenmode need be no larger than $1/N$th of the total space. A typical MOF with six fold rotational and reflection symmetry has, for example, a degenerate fundamental mode pair. If partitioned as prescribed above, the two modes have rotation numbers $l = \pm 1$, giving relations such as

$$E_z(\mathbf{R}_{\pi/3}\mathbf{r}) = \exp(\pm i\pi/3) E_z(\mathbf{r}) \qquad (l = \pm 1 \ \text{mode}). \tag{10}$$

One might think of the $(l = \pm 1)$ as circularly polarized modes, while quadrant-based class 3 and 4 modes are the corresponding linearly polarized superpositions. The fundamental can be calculated using one sixth of the space, with substantial savings over a quadrant. Further, when we replace the quadrant with rotation-number partitioning, we get a cleaner separation of all classes. For example, the quadrant-based calculation as described previously[13] fails to separate class 7 from class 3 modes without additional processing steps. Using rotational partitioning, class 3 modes $(l = 1)$ are separate from class 7 modes $(l = 3)$.

Further partitioning is possible for the nondegenerate modes, based on reflection symmetry. Classes 1, 2, 7, and 8 as described previously[13] already have the most efficient computational sectors. For these classes, each mode has the full rotational and reflection symmetry of the waveguide. This is tied to the nondegenerate nature of the modes[9] and depends on whether the flip operation maps a rotation class onto itself. For example, since the flip operation maps the $l = 1$ subspace onto the $l = -1$ subspace, it is clear that no mode of either subspace can have reflection symmetry. On the other hand, the $l = 0$ sector flips onto itself and can be partitioned into modes symmetric and antisymmetric upon reflection.

B. Implementation of Revised Classes

Quadrant symmetry for the fundamental mode has apparently been used in previous calculations not only using the multipole method,[9] but nearly all numerical methods, including finite element[11] and the efficient-modal method.[7] One recent vector wave expansion method is perhaps the only exception.[10] Quadrant-based methods result in larger matrix computations and fail to cleanly separate the classes; the quadrant method described in Ref. 13 finds modes of class 7 when searching for class 3 modes, class 8 when searching for 4, and so forth. This failure can lead to serious problems when modes of different classes have similar propagation constants.

Application of the proposed symmetry treatment to finite element and other methods should be extremely straightforward. In fact, the relevant symmetry operations have already been discussed in Table 1 and mode equations Eqs. (7) and (8). Implementing the symmetry reduction will require some care in defining the basic field representation. It is assumed in Table 1, for example, that the sampled grid of position vectors (finite element) or k vectors (plane wave) rotates onto itself. As discussed previously[17] (for similar reasons), the grid should be defined so that $\mathbf{Rr}$ is a grid point whenever $\mathbf{r}$ is.

It is worth noting that any effort spent on coding quadrant-based symmetry groups is not wasted. They are the most efficient partition for C_{2v} waveguides, such as dual-core couplers and various birefringent fiber designs.

4. EXAMPLE: MANY-MODED AIR-CORE FIBER

The advantages of the proposed symmetry implementation are now demonstrated with an air-core fiber example. For air-core fibers, accurate modeling of nearly degenerate modes is crucial even if single-mode operation is desirable, since unwanted glass-guided modes near the core are a major impairment.[8]

The multipole mode solver was used to calculate bandgap-confined modes of an air-core fiber with a three-ring cladding of holes (diameter $d = 2\,\mu$m, spacing $\Lambda = 2.5\,\mu$m) surrounding a circular air core. Figure 1 shows several calculated mode lines within the bandgap, along with a guideline (dashed) indicating the approximate index and slope we would expect from a fundamental core mode. This rough guideline can be obtained analytically simply by using solutions of a perfectly conducting waveguide of an appropriate size. The inflection of class 3 and 4 modes (bold lines) near the dashed line is characteristic of a core-confined fundamental mode,[18] as expected, but generally the mode structure is dominated by the unwanted glass-guided modes confined to the webs near the core. This is an example of a poor air-core design plagued by unwanted modes. The intensities for typical quasi-fundamental and a glass-guided modes are shown in Fig. 2 and clearly identify these as air-guided and glass-guided modes, respectively.

For such a multimode structure, failure to cleanly separate the mode classes can cripple the simulation. This is shown in the lower part of Fig. 1, where mode lines for an identical MOF structure have been calculating using an

identical mode-finding procedure, but using the quadrant-based symmetry classes for degenerate classes 3, 4, 5, and 6 instead of the $l = \pm 1, \pm 2$ versions. We see that the quadrant-based classes not only cause confusion at the crossing of mode lines (interrupting the quasi-fundamental mode line) but also lead to one mode line being entirely omitted (location shown by arrows).

To understand the problem, recall that the central calculation of the multipole mode solver is to find a matrix singularity. If vector **b** is a multipole representation of the field, the mode condition takes the form[13] $\mathbf{M}(\lambda, k_z)\mathbf{b} = 0$. A mode is identified by a dip in the singular value or determinant of **M** at $k_z = 2\pi n_{\text{eff}}/\lambda$. Figure 3 plots det(**M**) as a function of n_{eff} for several symmetry classes at wavelength $\lambda = 1.410$. The plot has several interesting features: First, the simulations confirm that the "quadrant" class 4 calculation is a composite of the class 8 and $(l = 2)$ calculation. The determinants are apparently related by simple multiplication: $|\det(\mathbf{M}_{4\text{quad}})| \approx |\det(\mathbf{M}_8)\det(\mathbf{M}_{l=1})|$. Second, we see that the combined class 4 makes it more difficult to extract information about the modes. A simple search for minima will overlook one of the two class 8 "dips." The quadrant-symmetry calculation is prone to overlooked modes and qualitatively inaccurate results, unless more sophisticated processing is applied.

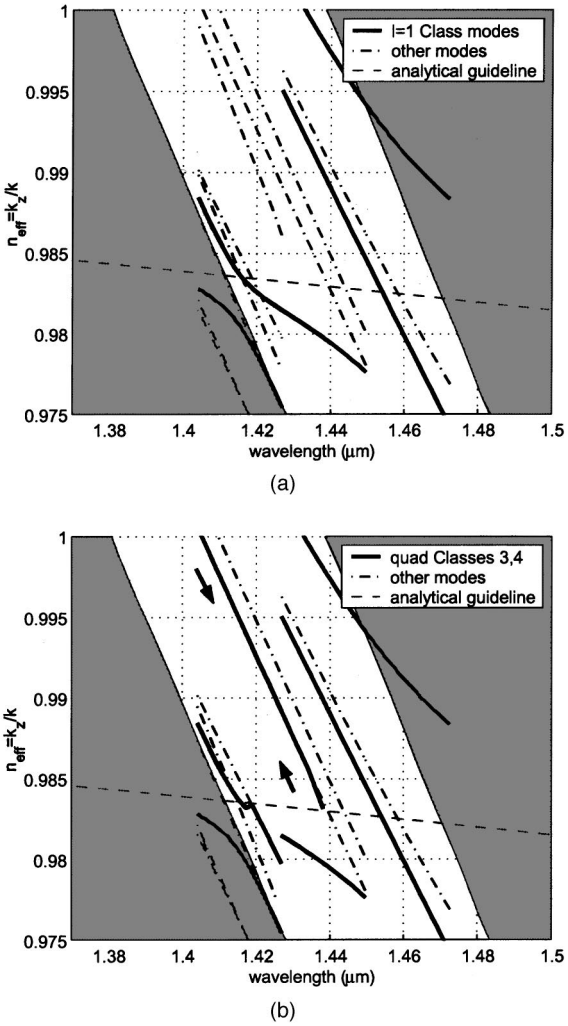

Fig. 1. Mode lines of this air-core microstructure fiber are shown in the region of the $\lambda - n_{\text{eff}}$ plot, where the bandgap (unshaded region) crosses $n_{\text{eff}} = 1$. Mode structure is primarily dominated by unwanted glass-guided modes.

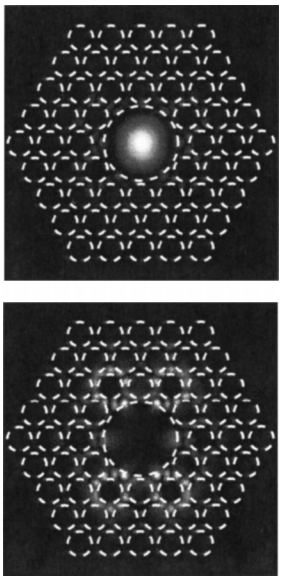

Fig. 2. Calculated intensity profiles show two modes with $n_{\text{eff}} \approx 0.98$, a fundamental core mode at $\lambda = 1.44$ (center), and a surface mode at $\lambda = 1.42$, guided primarily in glass webs (right). Holes are shown dashed.

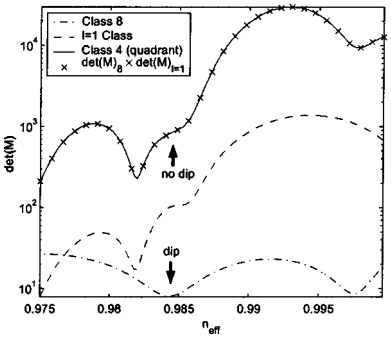

Fig. 3. Determinant of the mode-condition matrix is plotted versus n_{eff} for three subspaces: class 8, class 4 quadrant, and class 4 rotation $(l = 1)$. The product relation is indicated by the agreement between 'x' symbols and the solid curve.

The quadrant-based calculation fails, in part, because these particular modes are poorly confined and do not have sharp dips on the real-n_{eff} line. The problem is eliminated, in this case, if more rings of holes are added, giving lower-loss and sharper dips; however, this is at a much greater cost in CPU time. The cleaner symmetry separation, on the one hand, allows a quick preliminary mode analysis (of a smaller cladding) to guide a full, many-hole structure. On the other hand, other structures, including multicore fibers, will face even more severe difficulties without proper symmetry treatment because of a greater number of modes with similar effective indices.

Savings in computation time depend on various details of the calculation. In one example, calculating det(M) for all classes of a five-ring MOF structure gave a factor of 2 savings in computation time.

5. ROTATION-ONLY SYMMETRY EXAMPLE

Rotation-based symmetry reduction of simulations has one additional motivation: It can be used for structures that have rotational symmetry but no reflection symmetry. A final example with C_6 resembles the "satellite fiber" discussed previously,[9] an ordinary triangular-lattice fiber with additional small cylinders of high-index material included near the edge of the core region. Figure 4 shows the geometry and effective index plot of this fiber (right), compared with a similar fiber without the high-index inclusions (left). The unshaded region between the silica index (set to 1.45 for simplicity) and the effective cladding index (obtained from Bloch analysis) is available for index confinement in a silica core. The first higher-order mode group crosses from this confinement region to the shaded cladding-mode region.

The results for the satellite fiber agree with our physically intuitive understanding of this structure. At short wavelengths, the high-index regions act like individual stepindex cores (weakly coupled to each other and the air holes), and so the lowest-order mode lines converge to the well-known analytical solutions of a step-index fiber (shown dashed and labeled "SIF solution"). At long wavelengths, the tiny high-index regions become a small perturbation, and the mode lines approach the solutions of the simple two-ring MOF (shown in the left figure).

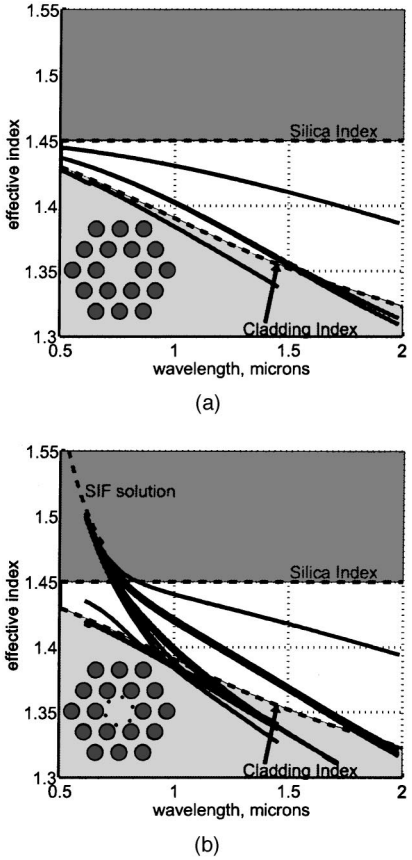

Fig. 4. Simulated effective index of a typical microstructure fiber (left) is compared with the similar "satellite fiber" (right), demonstrating the applicability of the revised symmetry classes to fibers with no reflection symmetry. Both fibers have a two-ring cladding of air holes with spacing $\Lambda = 2\ \mu$m and diameter $d = 1.3\ \mu$m. The satellite fiber includes small high-index inclusions at the periphery of the core region (index 2.0, radius $\approx 0.1\ \mu$m). The inclusions act as waveguides at short wavelengths and perturbations at long wavelengths.

For the C_6 structure, all six rotational symmetry classes are defined according to Table 1, not just the degenerate classes. This has the unfortunate result that the rotation classes with $l = 0$ and $l = 3$ can no longer be partitioned according to reflection parity. For example, the near degeneracy of the TE-like and TM-like modes can be a nuisance. This is inevitable since the structure fundamentally does not have reflection symmetry; it is not a product of the proposed symmetry classes. A number of approaches can be taken to distinguish these modes, when necessary.

6. CONCLUSIONS

A revised implementation of symmetry classes has been proposed for simulating the most common class of microstructure fibers, those of sixfold rotational and reflection symmetry. As demonstrated in an example air-core fiber simulation, the revised classes give important advantages in cleanly separating nearly degenerate modes of a multimode waveguide.

The application of the revised symmetry classes to several common mode-solving methods has been outlined in brief. Implementing the revision should be straightforward and present similar advantages to those demonstrated. In addition, once implemented, the revised classes allow simulation of rotationally symmetric structures with and without reflection symmetry, with no additional changes to the simulation codes. We have demonstrated application of such a multipole code to a "satellite" type fiber. This demonstrates that some additional design freedom can be obtained in searching for optimized structures, without moving to much slower simulations assuming no symmetry.

ACKNOWLEDGMENTS

We thank Brian Usner for his valuable help in developing our simulation tools and David DiGiovanni for useful conversations.

REFERENCES

1. P. Kaiser and H. W. Astle, "Low-loss single-matrial fibers made from pure fused silica," Bell Syst. Tech. J. **53**, 1021–1039 (1974).
2. P. Yeh, A. Yariv, and E. Marom, "Theory of Bragg fiber," J. Opt. Soc. Am. **68**, 1196–1201 (1978).
3. T. A. Birks, J. C. Knight, and P. S. J. Russell, "Endlessly single-mode photonic crystal fiber," Opt. Lett. **22**, 961–963 (1997).
4. N. Venkataraman, M. T. Gallagher, C. M. Smith, D. Müller, J. A. West, K. W. Koch, and J. C. Fajardo, "Low loss (13 db/km) air core photonic band-gap fibre," presented at the 28th European Conference on Optical Communication, Copenhagen, Denmark, September, 8–12, 2002.
5. K. Tajima, J. Zhou, K. Kurokawa, and K. Nakajima, "Low water peak photonic crystal fibres," presented at the 29th European Conference on Optical Communication, Rimini, Italy, September 22–24, 2003, paper Th4.1.6.

6. S. A. Diddams, D. J. Jones, J. Ye, S. T. Cundiff, and J. L. Hall, "Direct link between microwave and optical frequencies with a 300 thz femtosecond laser comb," Phys. Rev. Lett. **84**, 5102–5105 (2000).
7. T. M. Monro, D. J. Richardson, N. G. R. Broderick, and P. J. Bennett, "Holey optical fibers: an efficient modal model," J. Lightwave Technol. **17**, 1093–1102 (1999).
8. D. Müller, D. C. Allan, N. F. Borrelli, K. T. Gahagan, M. T. Gallagher, C. M. Smith, N. Venkataraman, and K. W. Koch, "Measurement of photonic band-gap fiber transmission from 1 to 3 μm and impact of surface mode coupling," in *Quantum Electronics and Lases Science*, Vol. 89 of OSA Trends in Optics and Photonics Series (Optical Society of America, Washington, D.C., 2003), paper QTuL2.
9. M. J. Steel, T. P. White, and L. C. Botten, "Symmetry and degeneracy in microstructured optical fibers," Opt. Lett. **26**, 488–490 (2001).
10. N. A. Issa and L. Poladian, "Vector wave expansion method for leaky modes of microstructured optical fibers," J. Lightwave Technol. **21**, 1005–1012 (2003).
11. A. Cucinotta, S. Selleri, L. Vincetti, and M. Zoboli, "Holey-fiber analysis through the finite-element method," IEEE Photon. Technol. Lett. **14**, 1530–1532 (2002).
12. A. Ferrando, E. Silvestre, J. J. Miret, and P. Andrés, "Full vector analysis of a realistic photonic crystal fiber," Opt. Lett. **24**, 276–278 (1999).
13. B. T. Kuhlmey, T. P. White, G. Renversez, D. Maystre, L. C. Botten, C. M. deSterke, and R. C. McPhedran, "Multipole methods for microstructured optical fibers. II. Implementation and results," J. Opt. Soc. Am. B **19**, 2331–2341 (2002).
14. N. Guan, S. Habu, K. Takenaga, K. Himeno, and A. Wada, "Boundary element method for analysis of holey optical fibers," J. Lightwave Technol. **21**, 1787–1792 (2003).
15. P. R. McIsaac, "Symmetry-induced modal characteristics of uniform waveguides. I. Summary of results," IEEE Trans. Microwave Theory Tech. **23**, 421–429 (1975).
16. C. Vassalo, "Circular Fourier analysis of full Maxwell equations for arbitrarily shaped dielectric waveguides—application to gain factors of semiconductor laser waveguides," J. Lightwave Technol. **8**, 1723–1729 (1990).
17. A. Peyrilloux, T. Chartier, A. Hideur, L. Berthelot, G. Mélin, S. Lempereur, D. Pagnoux, and P. Roy, "Theoretical and experimental study of the birefringence of a photonic crystal fiber," J. Lightwave Technol. **21**, 536–539 (2003).
18. J. Jasapara, R. Bise, T. Her, and J. Nicholson, "Effect of mode cut-off on dispersion in photonic bandgap fibers," *Optical Fiber Communication Conference*, Vol. 86 of OSA Trends in Optics and Photonics Series (Optical Society of America, Washington, D.C., 2003), paper ThI3.